Spontaneous Circulation of Confined Active Suspensions

Francis G. Woodhouse and Raymond E. Goldstein

Department of Applied Mathematics and Theoretical Physics, Centre for Mathematical Sciences, University of Cambridge, Wilberforce Road, Cambridge CB3 0WA, United Kingdom

(Received 22 July 2012; published 19 October 2012)

Many active fluid systems encountered in biology are set in total geometric confinement. Cytoplasmic streaming in plant cells is a prominent and ubiquitous example, in which cargo-carrying molecular motors move along polymer filaments and generate coherent cell-scale flow. When filaments are not fixed to the cell periphery, a situation found both *in vivo* and *in vitro*, we observe that the basic dynamics of streaming are closely related to those of a nonmotile stresslet suspension. Under this model, it is demonstrated that confinement makes possible a stable circulating state; a linear stability analysis reveals an activity threshold for spontaneous autocirculation. Numerical analysis of the longtime behavior reveals a phenomenon akin to defect separation in nematic liquid crystals and a high-activity bifurcation to an oscillatory regime.

DOI: 10.1103/PhysRevLett.109.168105 PACS numbers: 87.16.Wd, 47.54.−r, 47.63.−b, 87.16.Ln

Cytoplasmic streaming is the deliberate, driven motion of the entire contents of large eukaryotic cells. It is effected by cargo-laden molecular motors walking along polymer filaments and entraining the surrounding fluid [Fig. 1(a)]; the combined action of many of these motors can generate flow speeds in excess of 100 μm/s for certain freshwater algae. While inroads are being made into understanding its function [1,2], surprisingly little is known about how it is initially established within cells.

In a remarkable, yet apparently little-known investigation into the development of streaming, Yotsuyanagi [3] in 1953 examined isolated droplets of cytoplasm forcibly extracted from algal cells. He observed a progression from isolated Brownian fluctuations to a coherent, global circulation of the entire droplet contents [Fig. 1(b)]. However, we need not limit ourselves to *ex vivo* experiments: Kamiya [4] describes a similar blooming of rotational cyclosis in the development of *Lilium* pollen cells, and Jarosch [5] quantitatively analyzed the same disorder-to-order transition occurring within *Allium* cells over the course of a few hours. Based on these observations, one is led to ask: is it possible that a simple self-organization process could lie at the heart of streaming?

When the filaments are not locked in position, as is likely in Yotsuyanagi's experiments, a cargo-carrying motor walking on a free filament constitutes a force dipole. Therefore, these cytoplasmic dynamics belong to the burgeoning field of *active fluids*. With roots in self-organizing flocking models [6], an active fluid is a suspension of force dipoles interacting via short- and long-range forces: a system like a liquid crystal but with continuous injection of energy at the microscale. Such systems generically possess spontaneous flow instabilities [7] and can exhibit complex patterns and flows [8], including asters and vortices [9–11], laning [12,13], and density waves [11–13]. Spontaneous flow, in particular, is a key characteristic of flocking dynamics [6] and assumes an important role in applications such as cortex remodeling processes [14].

Despite the ubiquity of relevant situations, of which streaming is a major example, the influence of total confinement is relatively little-studied. Kruse *et al.* [9] included a finite domain in their study of single defect stability in polar gels, assuming perfect alignment everywhere bar the defect core, and found a dependence of aster and vortex stability on domain size. More recently, Schaller *et al.* [15] underlined the critical importance of long-range hydrodynamics in confined systems: swirling patterns were observed experimentally in a totally confined actin motility assay but were absent in cellular automaton simulations. They concluded that confined flows are responsible for the formation and stability of the global circulation. It seems reasonable, therefore, to posit that

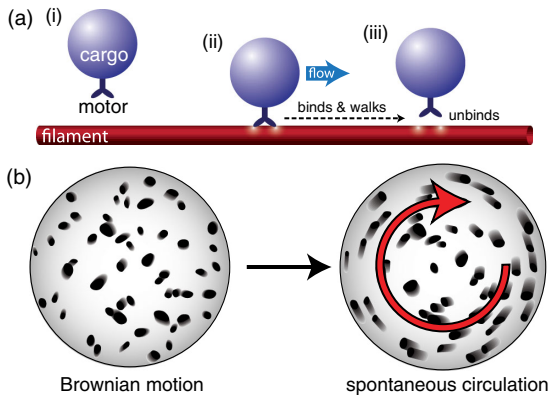

FIG. 1 (color online). Cytoplasmic streaming *in vivo* and *ex vivo*. (a) A molecular motor attached to a vesicle (i) encounters a filament, (ii) binds and walks along it, entraining fluid, before (iii) unbinding stochastically. (b) A drop of cytoplasm extracted from a plant cell transitions from random Brownian fluctuations to ordered circulation [3].

combining confinement with the spontaneous flow characteristics of active fluids will lead to circulatory streaming states. Indeed, such effects were taken advantage of by Fürthauer *et al.* [16] to construct theoretically a "Taylor-Couette motor," albeit in a geometry topologically distinct from a single confined chamber.

Through theory and simulation, we show here that the combination of confinement and activity allows for the emergence of stable self-organized rotational streaming. This is achieved using a ground-up approach employing closure techniques new to active suspension theory. Our model assumes that short, rigid filaments are suspended in a Newtonian, zero Reynolds number fluid, and that they exert extensile, or "pusher," dipolar forces on the fluid; this can be viewed as the effect of processive molecular motors landing randomly along a filament and walking toward one end, implying an average motor location forward of the filament midpoint. The suspension is taken to be dilute, so filaments interact via hydrodynamics only, and is confined within a no-slip sphere of diameter L.

Working in d dimensions, we generalize the standard kinetic approach to these systems [17]. The spatial and angular distribution function $\Psi(\mathbf{x}, \mathbf{p}, t)$ of the filaments, where $|\mathbf{p}| = 1$, satisfies a Smoluchowski equation

$$\frac{\partial \Psi}{\partial t} = -\boldsymbol{\nabla}_{\mathbf{x}} \cdot (\dot{\mathbf{x}}\Psi) - \boldsymbol{\nabla}_{\mathbf{p}} \cdot (\dot{\mathbf{p}}\Psi), \tag{1}$$

where $\boldsymbol{\nabla}_{\mathbf{x}} \equiv \partial/\partial\mathbf{x}$ and $\boldsymbol{\nabla}_{\mathbf{p}} \equiv (\mathbf{I} - \mathbf{pp}) \cdot \partial/\partial\mathbf{p}$. The spatial and rotational fluxes are

$$\dot{\mathbf{x}} \equiv \mathbf{u} + V\mathbf{p} - \mathsf{D}^{(s)} \cdot \boldsymbol{\nabla}_{\mathbf{x}} \log\Psi,$$
$$\dot{\mathbf{p}} \equiv (\mathbf{I} - \mathbf{pp}) \cdot (\gamma\mathsf{E} + \mathsf{W}) \cdot \mathbf{p} - D^{(r)}\boldsymbol{\nabla}_{\mathbf{p}} \log\Psi,$$

where V is a self-advection speed, $\gamma \in [-1, 1]$ is a shape parameter ($\gamma \to 1$ for a slender rod), $\mathsf{D}^{(s)}$ is a spatial diffusion tensor, and $D^{(r)}$ is a rotational diffusion constant. The fluid has velocity field $\mathbf{u}$, rate-of-strain tensor $\mathsf{E} \equiv (\boldsymbol{\nabla}\mathbf{u} + \boldsymbol{\nabla}\mathbf{u}^{\mathsf{T}})/2$, and vorticity tensor $\mathsf{W} \equiv (\boldsymbol{\nabla}\mathbf{u} - \boldsymbol{\nabla}\mathbf{u}^{\mathsf{T}})/2$. The filament pusher stresslet of strength $\sigma > 0$ generates a stress tensor $\boldsymbol{\Sigma} \equiv -\sigma \int_{\mathbf{p}} d\mathbf{p}(\mathbf{pp} - \mathbf{I}/d)\Psi$ that drives fluid flow by the Stokes equation $-\mu\nabla^2\mathbf{u} + \boldsymbol{\nabla}\Pi = \boldsymbol{\nabla} \cdot \boldsymbol{\Sigma}$ with viscosity μ and pressure Π, subject to incompressibility $\boldsymbol{\nabla} \cdot \mathbf{u} = 0$. Confinement induces the no-slip boundary condition $\mathbf{u} = 0$ on $|\mathbf{x}| = L/2$.

While simulations of the full system (1) are possible [17–19], here we develop evolution equations for the primary orientation moments [20–22]. Given the orientational average $\langle\phi\rangle \equiv \int_{\mathbf{p}} d\mathbf{p}\phi\Psi$, define the concentration $c \equiv \langle 1\rangle$, polar moment $\mathbf{P} \equiv \langle\mathbf{p}\rangle$, and nematic moment $\mathsf{Q} \equiv \langle\mathbf{pp} - \mathbf{I}/d\rangle$. Equations of motion for these fields in terms of higher moments can then be derived by taking appropriate weighted integrals of Eq. (1) [23].

We pare down complications by specializing to two dimensions ($d = 2$), rodlike particles ($\gamma = 1$), and isotropic diffusion ($\mathsf{D}^{(s)} = D^{(s)}\mathbf{I}$) and neglect self-advection ($V \equiv 0$). This last assumption decouples the c dynamics into pure advection diffusion and eliminates all polar interactions, so we take a constant concentration $c \equiv c_0$ and neglect $\mathbf{P}$. However, the remaining Q dynamics still depends on the fourth moment contraction $\langle\mathbf{pppp}\rangle$:$\mathsf{E}$, and a closure is needed. Typically, this is done by taking the distribution Ψ to be a functional purely of the first three moments, yielding a closure linear in Q [22]. In dense active systems, this is permissible, owing to the presence of local interaction terms in higher powers of Q; here, however, it is the above fourth moment term which provides all stabilizing nonlinearities, so greater care must be taken. Instead, we adopt a new approach by adapting a closure of Hinch and Leal [24] to $d = 2$, yielding

$$\langle\mathbf{pppp}\rangle:\mathsf{E} \approx \frac{1}{4c_0}[4\mathsf{Q} \cdot \mathsf{E} \cdot \mathsf{Q} + 2c_0(\mathsf{E} \cdot \mathsf{Q} + \mathsf{Q} \cdot \mathsf{E}) + c_0^2\mathsf{E} - 2\mathbf{I}\mathsf{Q}^2:\mathsf{E}].$$

This is derived in [24] as an interpolation between exact closures for the regimes of total order and disorder, giving a simple approximation to the hydrodynamic nonlinearities. After nondimensionalizing by rescaling $\mathbf{x} \to L\mathbf{x}$, $t \to (c_0L^2/\mu)t$, $\mathbf{u} \to (\mu/c_0L)\mathbf{u}$, $\Pi \to (\mu^2/c_0L^2)\Pi$, $\boldsymbol{\Sigma} \to (c_0L^2/\mu^2)\boldsymbol{\Sigma}$, and $\mathsf{Q} \to c_0\mathsf{Q}$, the final model reads

$$\frac{D\mathsf{Q}}{Dt} = d^{(s)}\nabla^2\mathsf{Q} - 4d^{(r)}\mathsf{Q} + \frac{1}{2}\mathsf{E} - 2\mathsf{Q} \cdot \mathsf{E} \cdot \mathsf{Q}, \tag{2}$$

where $D/Dt \equiv \partial/\partial t + \mathbf{u} \cdot \boldsymbol{\nabla}$, with nondimensional diffusion constants $d^{(s)} \equiv (c_0/\mu)D^{(s)}$ and $d^{(r)} \equiv (c_0L^2/\mu)D^{(r)}$. This is subject to the Stokes equation $-\nabla^2\mathbf{u} + \boldsymbol{\nabla}\Pi = -\sigma_0\boldsymbol{\nabla} \cdot \mathsf{Q}$ and incompressibility $\boldsymbol{\nabla} \cdot \mathbf{u} = 0$ with nondimensional dipole stress $\sigma_0 \equiv (c_0L/\mu)^2\sigma$. The fluid boundary condition reads $\mathbf{u} = 0$ on $|\mathbf{x}| = 1/2$. Among the variety of admissible boundary conditions on Q, we focus here on the *natural* condition $\mathbf{N} \cdot \boldsymbol{\nabla}\mathsf{Q} = 0$, where $\mathbf{N}$ is the boundary normal vector. Qualitatively similar results are found with fixed boundary-parallel or boundary-perpendicular conditions [23].

The model (2) has the structure of a Landau theory for the order parameter Q. As E is linear in the velocity $\mathbf{u}$, and $\mathbf{u}$ is (nonlocally) linear in $\sigma_0\mathsf{Q}$ via the Stokes equation, the term $(1/2)\mathsf{E} \propto \sigma_0\mathsf{Q}$. It follows in the usual manner that there is an effective linear term in Q that will become positive for sufficiently large activity σ_0 relative to $-4d^{(r)}$. If this is sufficient to overcome the diffusive stabilization $d^{(s)}$, then the amplitude of the ensuing instability will be limited by the nonlinear term $2\mathsf{Q} \cdot \mathsf{E} \cdot \mathsf{Q} \propto \mathsf{Q}^3$.

We first seek a steady nonflowing axisymmetric state Q^0. In polar coordinates $\alpha = (r, \theta)$, the tensor Laplacian of Q has primary components

$$(\nabla^2\mathsf{Q})_{r\alpha} = \mathcal{L}Q_{r\alpha} \equiv \frac{1}{r}\frac{\partial}{\partial r}\left(r\frac{\partial Q_{r\alpha}}{\partial r}\right) - \frac{4}{r^2}Q_{r\alpha},$$

while the others follow from symmetry and the tracelessness of Q. Equation (2) therefore implies Q^0_{rr} and $Q^0_{r\theta}$ each satisfy a (modified) Bessel equation in $z \equiv 2\Delta r$, viz. $z^2\partial_z^2 Q^0_{r\alpha} + z\partial_z Q^0_{r\alpha} - (z^2+4)Q^0_{r\alpha} = 0$, where $\Delta^2 \equiv d^{(r)}/d^{(s)}$. Thus, $Q^0_{r\alpha} \propto I_2(2\Delta r)$; since I_2 is monotonic, the boundary conditions imply $\mathsf{Q}^0 = 0$ everywhere.

Now, perturb axisymmetrically: let $\mathsf{Q} = \epsilon\mathsf{R}$, $\epsilon \ll 1$, and write $\mathbf{u} = \epsilon v\hat{\boldsymbol{\theta}}$ and $\mathsf{E} = \epsilon\mathbf{e}$ for the induced flow (which has no radial component by incompressibility). Seek an exponentially growing state such that $\partial_t\mathsf{R} = s\mathsf{R}$. Then, to $O(\epsilon)$, the perturbation obeys $s\mathsf{R} = d^{(s)}\nabla^2\mathsf{R} - 4d^{(r)}\mathsf{R} + \frac{1}{2}\mathbf{e}$. To determine $\mathbf{e}$, we employ the technique of Kruse *et al.* [9] and write the Stokes equation as $\boldsymbol{\nabla}\cdot(-\tilde{\Pi}\mathbf{I} + 2\mathbf{e} - \sigma_0\mathsf{R}) \equiv \boldsymbol{\nabla}\cdot\boldsymbol{\Sigma}^{\mathrm{tot}} = 0$. The r component determines $\tilde{\Pi}$. The θ component reads $\partial_r\Sigma^{\mathrm{tot}}_{r\theta} + (2/r)\Sigma^{\mathrm{tot}}_{r\theta} = 0$, so, for $\Sigma^{\mathrm{tot}}_{r\theta}$ analytic at $r = 0$, we find $\Sigma^{\mathrm{tot}}_{r\theta} = 0$, i.e., $e_{r\theta} = (\sigma_0/2)R_{r\theta}$. Finally, $e_{rr} = 0$, as there is no radial velocity component. The perturbation therefore satisfies

$$d^{(s)}\mathcal{L}R_{rr} = (4d^{(r)} + s)R_{rr}, \tag{3}$$

$$d^{(s)}\mathcal{L}R_{r\theta} = \left(4d^{(r)} + s - \frac{\sigma_0}{4}\right)R_{r\theta}, \tag{4}$$

which are still of Bessel form. When $s > -4d^{(r)}$, Eq. (3) has a solution in terms of I_2, so boundary conditions imply $R_{rr} = 0$. Now, let $\lambda \equiv (4d^{(r)} + s - \sigma_0/4)/d^{(s)}$ and write Eq. (4) as $\mathcal{L}R_{r\theta} = \lambda R_{r\theta}$. For $\lambda > 0$, this again gives solutions in terms of I_2, and so $R_{r\theta} = 0$. However, for $\lambda < 0$ (i.e., sufficiently large σ_0), the solution is instead $R_{r\theta} \propto J_2(\sqrt{-\lambda}r)$. Applying the boundary condition $R'_{r\theta}(1/2) = 0$ yields the eigenvalue $\lambda = -4y_0^2$ in terms of $y_0 \approx 3.054$, the first positive point satisfying $J_2'(y_0) = 0$. This implies that the homogeneous disordered state is unstable to a spontaneously flowing mode when $\sigma > \sigma^*$, where (in physical units)

$$\sigma^* \simeq \frac{16\mu}{c_0}\left(9.33\frac{D^{(s)}}{L^2} + D^{(r)}\right), \tag{5}$$

which we verified numerically by simulations of Eq. (2).

Stability analysis in the unbounded case elicits instability of a long-wavelength band when $\sigma_0 > 16d^{(r)}$ (see also [17]), compatible with the $L \to \infty$ limit of Eq. (5). This illustrates the action of confinement as a strong constraint on the available excitation modes, allowing for selection of a single circulation mode as opposed to a band of wave numbers. Similar spontaneous flows have been observed in active nematic models under periodic conditions [13], but the excited modes exhibit "laning" flows, as opposed to the circulation seen here. To lend perspective, we consider typical values of the material properties. The stress amplitude can be expressed as $\sigma = f\ell$, where f is the (typically pN) force exerted by motors and ℓ is the (typically μm) separation of the opposing forces of the stresslet. For micron-size rods, we expect $D^{(r)} \sim 0.01\ \mathrm{s}^{-1}$ and $D^{(s)} \sim 10^{-9}\ \mathrm{cm}^2/\mathrm{s}$, so, for system sizes $L \gtrsim 10\ \mu$m, rotational diffusion dominates in Eq. (2). Then, for a fluid of the viscosity of water in an idealized slab geometry, the instability will set in at $c_0 \gtrsim 10^8\ \mathrm{cm}^{-3}$, corresponding to a volume fraction well below 10^{-3}.

In order to confirm that the circulating configuration is steady at long times, we must turn to simulations of the fully nonlinear dynamics. In the following numerical studies, we vary the dipolar activity σ_0 while fixing the diffusion constants at $d^{(r)} = d^{(s)} = 0.025$ and use the eigendecomposition $\mathsf{Q} = S(\mathbf{nn} - \mathbf{I}/2)$, where the order parameter S and (headless) director $\mathbf{n}$ are the degree of local alignment

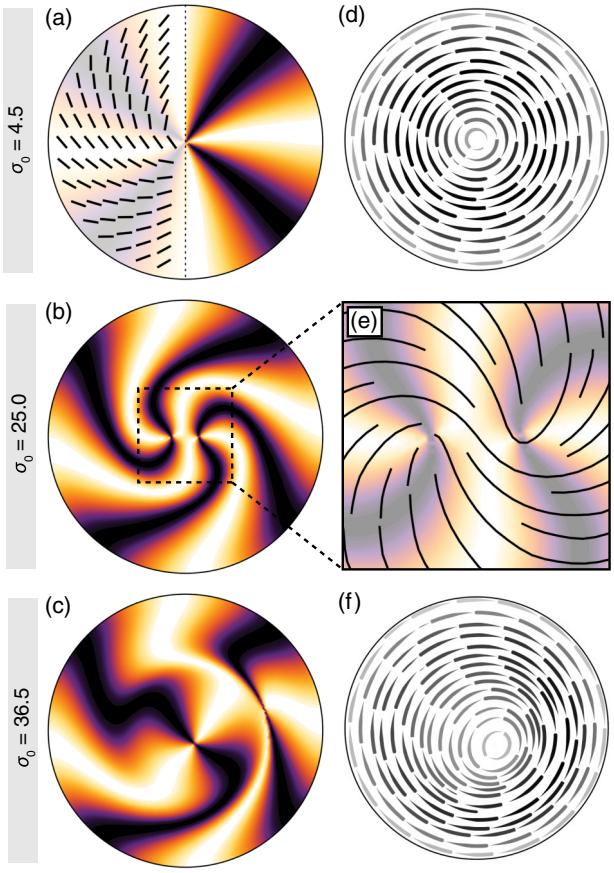

FIG. 2 (color online). Numerical results beyond the spontaneous circulation threshold. (a),(b),(c) Simulated schlieren textures of nematic order director $\mathbf{n}$ [i.e., density plot of $(n_x n_y)^2$]. Lighter shades correspond to diagonally oriented filaments, darker shades to horizontal or vertical filaments. (a) Steady circulation with a central spiral defect at low activity (the left overlay shows order field $\mathbf{n}$), (b) steady central defect separation into a pair of hyperbolic defects, and (c) snapshot of oscillatory behavior with widely separated mobile defects. (d) Flow streamlines for low activity, showing circulation about the system center; darker streamlines indicate faster flow. (e) Enlargement of the nematic director field structure in texture (b), showing two hyperbolic defects. (f) Flow streamlines for high-activity oscillation associated with texture (c), exhibiting off-center flow circulation. In all cases, $d^{(r)} = d^{(s)} = 0.025$.

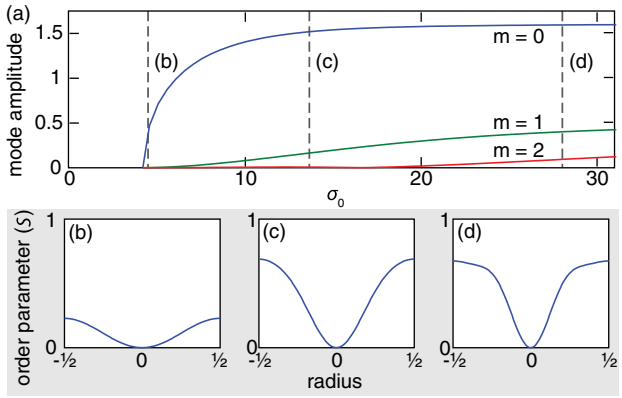

FIG. 3 (color online). Details of the bifurcation to circulation. (a) Numerically evaluated steady-state amplitudes $|S_0^{(m)}|$ of Bessel series expansion for the axisymmetric part of the order parameter S at varying activity σ_0, with $d^{(r)} = d^{(s)} = 0.025$. (b)–(d) Profiles of S at indicated points (b)–(d) in (a).

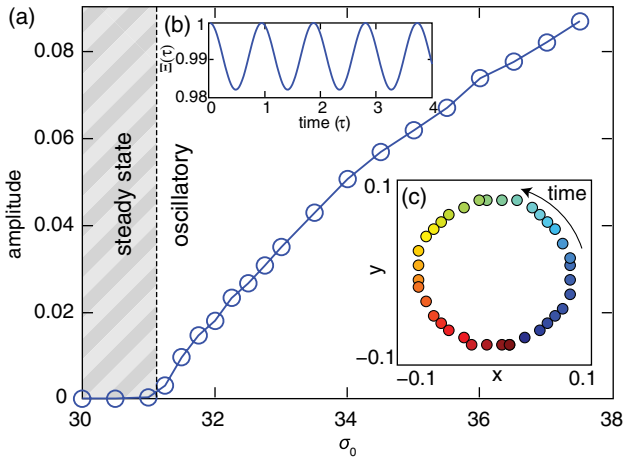

FIG. 4 (color online). Secondary bifurcation to oscillatory dynamics. (a) Amplitude of oscillation of the velocity correlation function $\Xi(\tau)$ vs σ_0, with $d^{(r)} = d^{(s)} = 0.025$, showing a bifurcation from steady defect separation to oscillatory behavior at a critical value of σ_0. (b) $\Xi(\tau)$ for $\sigma_0 = 32$, showing periodic oscillatory behavior. (c) Position of the flow circulation center over time for $\sigma_0 = 32.75$ during one oscillation period.

and the average alignment direction, respectively. For sufficiently weak activity above σ^*, a stable steady state emerges of circulation about the system center [Figs. 2(a) and 2(d)]. The spiral pattern of the nematic director field is reminiscent of the predictions of Kruse *et al.* [9] for polar systems (see also [10,25]). Higher mode contributions can be examined by expanding the order parameter as $S(r,\theta) = \sum_n S_n(r)e^{in\theta}$ and applying an appropriate $n = 0$ mode expansion $S_0(r) = \sum_{m=0}^{\infty} S_0^{(m)} J_2(2y_m r)$, where $J_2'(y_m) = 0$ and $y_m < y_{m+1}$. Mode amplitudes can then be extracted using orthogonality of the radial basis. Figure 3 shows the steady-state values of the first three amplitudes $|S_0^{(m)}|$ as functions of σ_0.

At larger values of σ_0, the steady state exhibits *defect separation*: the central axisymmetric spiral defect in the nematic director field (with topological charge $+1$) splits into two closely spaced hyperbolic defects (each of charge $+1/2$), illustrated in Figs. 2(b) and 2(e). The system still possesses fluid circulation about the central axis, due to the symmetric positioning of the defects. Defect separation is perhaps unsurprising if we make contact with liquid crystal theory; for approximately isolated defects, the free energy penalty per defect is proportional to the square of its topological charge [26], rendering two $+1/2$ defects favorable over a single $+1$ spiral. Indeed, de las Heras *et al.* [27] recently investigated the equivalent confined setup for a microscopic two-dimensional liquid crystal and always encountered defect separation.

As σ_0 is increased beyond a new critical value, the steady state is unstable and the system bifurcates into a regime of *periodic oscillation*, where the time symmetry is broken. The $+1/2$ defect pair [Fig. 2(c)] execute periodic "orbits" around each other, with the flow circulation center offset from the origin [Fig. 2(f)], following a quasicircular trajectory [Fig. 4(c)]. These states can be analyzed by examining the correlation function [15]

$$\Xi(\tau) \equiv \left\langle \frac{\langle \mathbf{v}(\mathbf{x},t)\cdot\mathbf{v}(\mathbf{x},t-\tau)\rangle_{\mathbf{x}}}{\langle \mathbf{v}(\mathbf{x},t)\cdot\mathbf{v}(\mathbf{x},t)\rangle_{\mathbf{x}}} \right\rangle_t,$$

where the temporal average is taken over late times when the oscillatory state is fully established. Extracting the amplitude A of oscillation of Ξ [Fig. 4(b)], we numerically determine a bifurcation diagram as a function of σ_0, as in Fig. 4(a). There is a clear threshold for the onset of periodic oscillations. A similar oscillatory bifurcation has been observed by Giomi *et al.* [13] for a dense active nematic in a channel geometry, suggesting that such behavior may be a fundamental property of active nematics, although the exact form taken will be heavily dependent on geometry and topology. Were this system an annulus, rather than a disk, behavior more closely resembling the "back and forth" oscillations of [13] could be conjectured as a regime beyond the spontaneous flow of [16].

Motivated by principles of cytoplasmic streaming, we have constructed a clean, simple model for a dilute suspension of extensile force-generating filaments in total geometric confinement and have demonstrated that inclusion of elementary hydrodynamics is entirely sufficient to yield spontaneous self-organization, in spite of the absence of more complex local interaction terms. In an experimental realization, the prediction of a critical activity for transition from quiescence to circulation can be tested by varying the viscosity or motor activity, perhaps through temperature or adenosine triphosphate (ATP) concentration. Modern realizations of Yotsuyanagi's experiment could provide a wealth of information on this type of bifurcation.

We thank S. Ganguly, E. J. Hinch, A. Honerkamp-Smith, P. Khuc Trong, and H. Wioland for discussions. This work was supported by the EPSRC and European Research Council Advanced Investigator Grant No. 247333.

[1] J. Verchot-Lubicz and R. E. Goldstein, Protoplasma **240**, 99 (2010).
[2] R. E. Goldstein, I. Tuval, and J. W. van de Meent, Proc. Natl. Acad. Sci. U.S.A. **105**, 3663 (2008).
[3] Y. Yotsuyanagi, Cytologia **18**, 146 (1953); **18**, 202 (1953).
[4] N. Kamiya, *Protoplasmic Streaming* (Springer-Verlag, Berlin, 1959).
[5] R. Jarosch, Protoplasma **47**, 478 (1956).
[6] T. Vicsek, A. Czirók, E. Ben-Jacob, I. Cohen, and O. Shochet, Phys. Rev. Lett. **75**, 1226 (1995); J. Toner and Y. Tu, Phys. Rev. E **58**, 4828 (1998); J. Toner, Y. Tu, and S. Ramaswamy, Ann. Phys. (N.Y.) **318**, 170 (2005).
[7] R. A. Simha and S. Ramaswamy, Phys. Rev. Lett. **89**, 058101 (2002).
[8] R. Voituriez, J. F. Joanny, and J. Prost, Europhys. Lett. **70**, 404 (2005).
[9] K. Kruse, J. F. Joanny, F. Jülicher, J. Prost, and K. Sekimoto, Phys. Rev. Lett. **92**, 078101 (2004).
[10] J. Elgeti, M. E. Cates, and D. Marenduzzo, Soft Matter **7**, 3177 (2011).
[11] K. Kruse, J. F. Joanny, F. Jülicher, J. Prost, and K. Sekimoto, Eur. Phys. J. E **16**, 5 (2005).
[12] L. Giomi and M. C. Marchetti, Soft Matter **8**, 129 (2012).
[13] L. Giomi, L. Mahadevan, B. Chakraborty, and M. F. Hagan, Phys. Rev. Lett. **106**, 218101 (2011); Nonlinearity **25**, 2245 (2012).
[14] G. Salbreux, J. Prost, and J. F. Joanny, Phys. Rev. Lett. **103**, 058102 (2009).
[15] V. Schaller, C. Weber, C. Semmrich, E. Frey, and A. R. Bausch, Nature (London) **467**, 73 (2010).
[16] S. Fürthauer, M. Neef, S. W. Grill, K. Kruse, and F. Jülicher, New J. Phys. **14**, 023001 (2012).
[17] D. Saintillan and M. J. Shelley, Phys. Fluids **20**, 123304 (2008); Phys. Rev. Lett. **100**, 178103 (2008).
[18] C. Helzel and F. Otto, J. Comput. Phys. **216**, 52 (2006).
[19] A. A. Pahlavan and D. Saintillan, Phys. Fluids **23**, 011901 (2011).
[20] M. Doi and S. F. Edwards, *The Theory of Polymer Dynamics* (Oxford University Press, New York, 1988).
[21] P. G. de Gennes and J. Prost, *The Physics of Liquid Crystals* (Clarendon, Oxford, 1995).
[22] A. Baskaran and M. C. Marchetti, Phys. Rev. E **77**, 011920 (2008).
[23] F. G. Woodhouse and R. E. Goldstein (unpublished).
[24] E. J. Hinch and L. G. Leal, J. Fluid Mech. **76**, 187 (1976).
[25] D. Marenduzzo and E. Orlandini, Soft Matter **6**, 774 (2010).
[26] T. Lubensky and J. Prost, J. Phys. II (France) **2**, 371 (1992).
[27] D. de las Heras, E. Velasco, and L. Mederos, Phys. Rev. E **79**, 061703 (2009).